ISSN 1674-1056
http://cpb.iphy.ac.cn
http://iopscience.iop.org/cpb
中国物理 B
Chinese Physics
中国物理 Chinese Physics B

A theoretical study of a plasmonic sensor comprising a gold nano-disk array on gold film with an SiO_2spacer

Xiangxian Wang(王向贤), Jiankai Zhu(朱剑凯), Huan Tong(童欢), Xudong Yang(杨旭东), Xiaoxiong Wu(吴枭雄), Zhiyuan Pang(庞志远), Hua Yang(杨华), Yunping Qi(祁云平)

Citation: Chin. Phys. B . 2019, 28(4): 044201. **doi:** 10.1088/1674-1056/28/4/044201
Journal homepage: http://cpb.iphy.ac.cn; http://iopscience.iop.org/cpb

What follows is a list of articles you may be interested in

Analysis of optical properties of bio-smoke materials in the 0.25-14 μm band

Xinying Zhao(赵欣颖), Yihua Hu(胡以华), Youlin Gu(顾有林), Xi Chen(陈曦), Xinyu Wang(王新宇), Peng Wang(王鹏), Xiao Dong(董骁)

Chin. Phys. B . 2019, 28(3): 034201. **doi:** 10.1088/1674-1056/28/3/034201

Cascaded tilted fiber Bragg grating for enhanced refractive index sensing

Biqiang Jiang(姜碧强), Zhixuan Bi(毕芷瑄), Shouheng Wang(王守恒), Teli Xi(席特立), Kaiming Zhou, Lin Zhang, Jianlin Zhao(赵建林)

Chin. Phys. B . 2018, 27(11): 114220. **doi:** 10.1088/1674-1056/27/11/114220

Coherently induced grating in refractive index enhanced medium

Zhuan-Zhuan Liu(刘撰撰), Yu-Yuan Chen(陈煜远), Jia-Yu Yuan(原佳宇), Ren-Gang Wan(万仁刚)

Chin. Phys. B . 2017, 26(12): 124209. **doi:** 10.1088/1674-1056/26/12/124209

Apodized grating coupler using fully-etched nanostructures

Hua Wu(武华), Chong Li(李冲), Zhi-Yong Li(李智勇), Xia Guo(郭霞)

Chin. Phys. B . 2016, 25(8): 084212. **doi:** 10.1088/1674-1056/25/8/084212

Optical control of light propagation in photonic crystal based on electromagnetically induced transparency

Dan Wang(王丹), Jin-Ze Wu(武晋泽), Jun-Xiang Zhang (张俊香)

Chin. Phys. B . 2016, 25(6): 064202. **doi:** 10.1088/1674-1056/25/6/064202

A theoretical study of a plasmonic sensor comprising a gold nano-disk array on gold film with a SiO_2 spacer*

Xiangxian Wang(王向贤)[1,†], Jiankai Zhu(朱剑凯)[1], Huan Tong(童欢)[1], Xudong Yang(杨旭东)[1], Xiaoxiong Wu(吴枭雄)[1], Zhiyuan Pang(庞志远)[1], Hua Yang(杨华)[1], and Yunping Qi(祁云平)[2]

[1] *School of Science, Lanzhou University of Technology, Lanzhou* 730050, *China*
[2] *College of Physics and Electronic Engineering, Northwest Normal University, Lanzhou* 730070, *China*

(Received 30 October 2018; revised manuscript received 9 January 2019; published online 19 March 2019)

A plasmonic refractive index (RI) sensor with high RI sensitivity based on a gold composite structure is proposed. This composite structure is constructed from a perfect gold nano-disk square array on a gold film, with a SiO_2 spacer. The reflection spectra of the composite structure, with analyte RI in the range of 1.30 to 1.40, are theoretically studied using the finite-difference time-domain method. The incident light beam is partly coupled to the localized surface plasmons (LSP) of the single nano-disks and partly transferred to the propagating surface plasmons (PSP) by grating coupling. The reflectivity is nearly zero at the valley of the reflection spectrum because of the strong coupling between LSP and PSP. Also, the full width at half maximum (FWHM) of one of the surface plasmon polaritons (SPPs) modes is very narrow, which is helpful for RI sensing. An RI sensitivity as high as 853 nm/RIU is obtained. The influence of the structure parameters on the RI sensitivity and the sensor figure of merit (FOM) are investigated in detail. We find that the sensor maintains high RI sensitivity over a large range of periods and nano-disk diameters. Results of the theoretical simulation of the composite structure as a plasmonic sensor are promising. Thus, this composite structure could be extensively applied in the fields of biology and chemistry.

Keywords: plasmonic sensor, refractive index, sensitivity, FOM

PACS: 42.25.–p, 42.70.–a, 42.79.–e **DOI:** 10.1088/1674-1056/28/4/044201

1. Introduction

As an important branch of nanophotonics, the surface plasmonics has received extensive attention in physics, materials science, nanotechnology, and other physical fields. The unique optical properties caused by surface plasmon polaritons (SPPs) have broad application prospects in photocatalysis,[1–5] photolithography,[6–8] nanoscale light manipulation,[9,10] absorption enhancement,[11,12] surface-enhanced Raman scattering,[13–15] and terahertz plasma waves.[16–18] The SPPs occur chiefly in the surface regions of metals as a result of intense interactions of photons and free electrons. In essence, SPPs are a kind of electromagnetic motion mode. Another practical application of SPPs is in chemical and biomedical sensing.[19–25] The variation in the refractive index (RI) of the surface plasmon evanescent field affects the propagation constant of SPPs and the position of the resonance wavelength. Therefore, SPPs are exceedingly sensitive to the RI of the surrounding environment. Numerous plasmonic RI sensors based on various sub-wavelength metallic particles and structures have been put forward because of this characteristic. In addition, plasmonic sensors have many advantages such as small sample sizes, being label-free,[26] real-time dynamic monitoring,[27,28] and a wide range of application fields.

Plasmonic sensors can be roughly classified into two categories: propagating surface plasmon (PSP) sensors excited by prism coupling[29–31] or grating coupling[32] and localized surface plasmon (LSP) sensors excited by nanoparticles or nanoholes. In previous work, plasmonic sensors based on nanospheres, nanorods, nanopyramids, and even nanostars[33–35] have been unable to achieve high RI sensitivity or good figure of merit (FOM) performance. In 2012, Huang *et al.* designed a sensor for DNA detection using randomly distributed gold nanorings and achieved a sensitivity of 350 nm/refractive index unit (RIU) and an FOM of 3.1 RIU^{-1}.[36] In 2013, Zhang *et al.* utilized the coupling of SPP modes and LSP modes to successfully reduce the full width at half maximum (FWHM) and obtained a sensitivity of 317 nm/RIU and an FOM of 8.3 RIU^{-1}.[37] In 2018, Wang *et al.* synthetically fabricated a periodic gold nanoring array and studied its structure parameters. The sensitivity of the array was measured to be 544 nm/RIU and the FOM was 6 RIU^{-1}.[38] With the continuous upgrading of lithography technology, more complex structures can be realized. For plasmonic sensors, these novel structures[39–45] are certain to have potential for RI sensor applications, and some of them may provide higher RI sensitivity and better FOM.

*Project supported by the National Natural Science Foundation of China (Grant Nos. 61865008 and 61505074), the Undergraduate Innovation Training Program of Gansu Province, China (Grant No. DC2018002), and the Undergraduate Innovation Training Program of Lanzhou University of Technology (Grant No. DC2018004).

†Corresponding author. E-mail: wangxx869@126.com

© 2019 Chinese Physical Society and IOP Publishing Ltd

In this paper, to obtain a plasmonic sensor with both a high RI sensitivity and a good FOM, a two-dimensional (2D) grating nano-disk array and gold film are utilized to form a composite structure. The PSPs and LSPs are both excited in this composite structure and the coupling strength is related to the structure parameters. The finite-difference time domain (FDTD) method is adopted to analyze the proposed design. The simulation results of the reflection spectra demonstrate that the resonance wavelength is sensitive to the RI and the FWHM of the resonance peak is narrow. Then, with a detailed discussion of the geometric parameters of the structure, we develop an approach to further enhance the RI sensitivity.

2. Sketch of the structure and theoretical methods

The three-dimensional schematics of the structure are shown in Fig. 1(a). From top to bottom, the components are gold nano-disk arrays, SiO_2 spacers, gold film, and a glass substrate. The square arrays are periodically extended along the x direction and y direction. Figure 1(b) presents a top-down view of the structure. The period is defined as the red lines in Fig. 1(b), which join the centers of two nearest neighbor nano-disks. All the nano-disks are of equal height (40 nm) and the diameter of the nano-disks is allowed to vary within a certain range. The thickness of the SiO_2 is 24 nm, and this is used for separating the disk arrays and the gold film, in order to excite strong coupling between localized and propagating surface plasmons. The thickness of the gold planar film is 100 nm and the whole structure resides on a glass substrate.

In this work, we use the FDTD method, which is widely used in optical simulations,[46–50] to calculate the reflection spectra of our structure. As shown in Fig. 1(a), the structure is irradiated by a plane wave with the polarization along the x direction at normal incidence from the upper side. Considering that the structure is periodic, we select the black foursquare lattice as the calculation unit, as shown in Fig. 1(b). The calculation unit is square, and the length of its sides is twice the period. Periodic boundary conditions are applied at the four side boundaries around the unit, and perfectly matched layer absorbing boundary conditions are used at the upper and lower boundaries. In this simulation, the RI of the gold is wavelength-dependent and the Drude model[51] is used for characterizing its dielectric constant, as shown in the following equation (1).

$$\varepsilon_\omega = 1 - \frac{\omega_p^2}{\omega(\omega + i\omega_c)}, \tag{1}$$

where the plasma frequency is $\omega_p = 2\pi \times 2.175 \times 10^{15}$ Hz, and the scattering frequency for bulk gold is $\omega_c = 2\pi \times 6.49 \times 10^{14}$ Hz.[52]

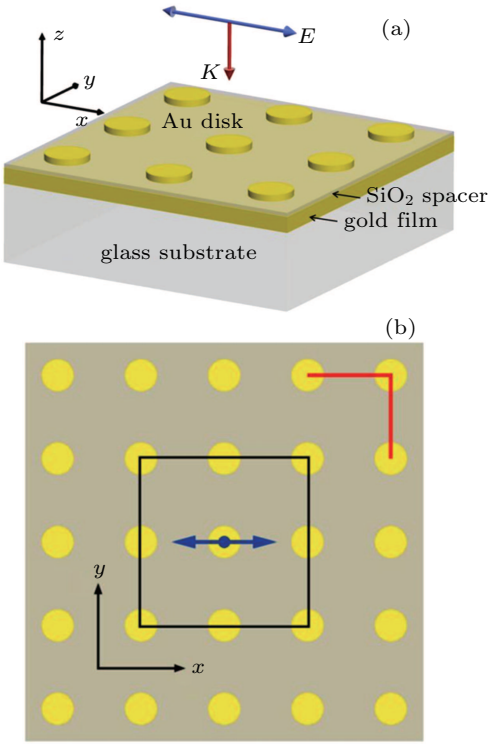


Fig. 1. (a) A schematic diagram of the composite structure, consisting of a perfect gold nano-disk square array on a gold film, with a SiO_2 spacer (the red arrow indicates the direction of propagation and the blue arrow indicates the polarization direction). (b) A top-down view of the structure. The black foursquare lattice is the calculation unit and the red line is the period.

3. Results and discussion

3.1. Theoretical analysis of the structure

Figure 2(a) shows the reflection spectrum of the structure simulated by the FDTD method in a wide wavelength range, from 500 nm to 2000 nm. In this case, the diameter of the nano-disks is 280 nm, the period is 720 nm, and the background index (analyte refractive index) is 1.30. As shown in the figure, three main resonant reflection modes can be found in the curve, located at 740 nm (mode 1), 964 nm (mode 2), and 1453 nm (mode 3). It is apparent that the surface plasmon polaritons can be effectively excited in this composite structure. The incident energy is coupled to LSP via single nano-disks, which interact with adjacent disks both in the upper space and through PSP. In addition, the incident energy is transferred to PSP via the two-dimensional (2D) grating. Furthermore, coupling between LSP and PSP enhances the energy of incident light transfer to SPPs.[53] The strong coupling results in very low reflectivity of the reflection spectrum at resonant wavelength. The nano-disk array acts as a 2D grating, which provides additional momentum and couples the incident plane wave into PSP. The additional momentum is given by the following equation[54,55]

$$G = \frac{2\pi}{d}\sqrt{n^2 + m^2}, \tag{2}$$

where d is the period constant and n and m are integers. As shown in Fig. 2(a), mode 1 and mode 2 correspond to (1, 1)

and (1, 0), respectively, and localized surface plasmons are predominant in the last resonant mode.[54]

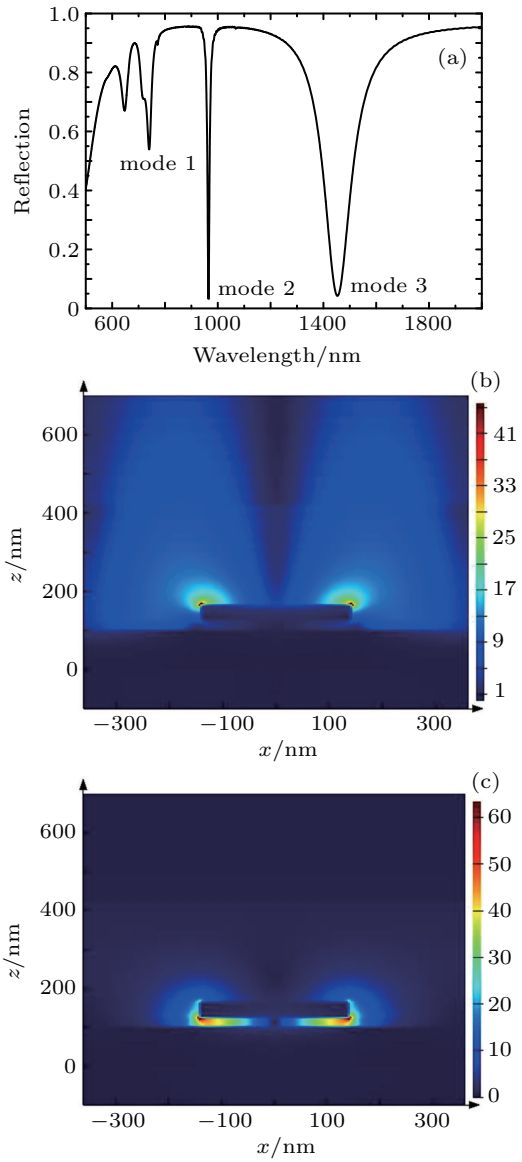


Fig. 2. (a) The reflection spectrum of the composite structure, where the period is 720 nm and the diameter of the nano-disks is 280 nm. Simulated electric field $|E|/|E_0|$ of mode 2 (b) and mode 3 (c) on the xz plane, along the diameter of the nano-disk.

To further examine the structural features, we calculated the electric-field distribution of mode 2 and mode 3 on the xz plane, along the diameter of the nano-disk. As shown in Figs. 2(b) and 2(c), the existence of SPPs is clearly indicated, and the electric-field enhancement in modes 2 and 3 is caused by strong coupling between LSP and PSP. It is noteworthy that both mode 2 and mode 3 are the result of LSP and PSP coupling. The main difference between them is that mode 2 is dominated by PSP, whereas mode 3 is dominated by LSP.

3.2. Sensing performance of the structure

This is how our structure works as a reflective index sensor. The change in the analyte RI on top of the arrays causes a resonance peak shift, and the analyte RI can be sensed by detecting the position of the resonance peak. The RI sensitivity and the FOM are often used for quantifying the performance of a reflective index sensor. A good RI sensor should have both high sensitivity and a high FOM. The RI sensitivity is defined as $S = \Delta\lambda/\Delta n$ ($\Delta\lambda$ is the shift of the resonance peak wavelength and Δn is the refractive index change of the analyte) and the FOM is defined as FOM = S/FWHM. As shown in Fig. 2(a), mode 1 is insufficient for RI sensing due to its weak resonance intensity (the reflectivity is around 0.5), compared with other resonance modes. Modes 2 and 3 have almost the same strong resonance intensity (the reflectivity is around 0). However, the FWHM of modes 2 and 3 is approximately 9 nm and 122 nm, respectively. Considering the relationship between the FOM and the FWHM (a small FWHM results in a high FOM), it is reasonable to choose mode 2 as the sensing peak, as it has the narrowest line width and therefore the better resonance intensity.

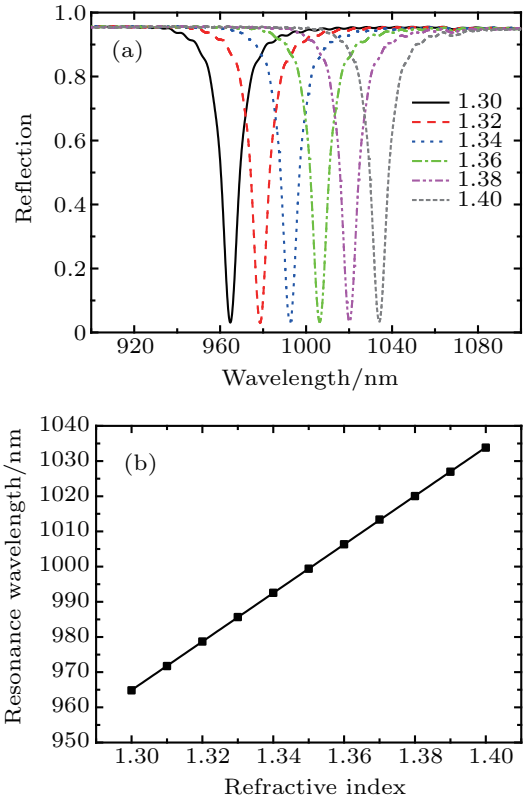


Fig. 3. (a) The reflection spectra of the same composite structure with different analyte RI. (b) The position of the resonance wavelength (mode 2) as a function of the RI.

Thus, we selected mode 2 to be our research object and we examine the near infrared wavelength range from 900 nm to 1100 nm (where mode 2 belongs), to study the influence of the analyte RI on the resonance mode. Six reflection spectra with different analyte RI and the same structure parameters are presented in Fig. 3(a). From these curves, we find that the resonance peaks show red shifts as the RI increases, and all the

spectra have almost the same FWHM and dip depths. This is because a slight change in the reflective index does not affect the resonance mechanism of surface plasmon polaritons in the structure. A good linear relationship (between the position of mode 2 and the RI of the analyte) is observed in Fig. 2(b). In order to calculate the sensitivity and the FOM, we plot the position of mode 2 as a function of the analyte RI in Fig. 3(b). The sensitivity and the FOM are calculated to be 690 nm/RIU and 76.6 RIU^{-1}, respectively, for a period of 720 nm and a diameter of 280 nm. The FOM of this plasmonic sensor is quite high compared to those of other plasmonic RI sensors[24–29] because of the narrow line width. However, this is not the best possible performance of the sensor. The sensor can be optimized by regulating some of the structure parameters to achieve a higher sensitivity, as discussed below. Thus, our sensor does not have strict structure parameter requirements and is able to work in a relatively rough process.

3.3. Influence of the period on the sensitivity and FOM

When the period is fixed, the resonance peaks change approximately linearly with the RI of the analyte and the sensitivity is fixed, according to the definition of sensitivity. Therefore, we investigated the sensitivity of plasmonic sensors of different periods, to determine the relationship between them. An interesting phenomenon was observed. When the period was increased, the position of the resonance wavelength (mode 2) changed evenly with the red shift. This provides a way of controlling the RI sensor. By changing the period to an appropriate size, we can choose the infrared band needed to detect the RI of the analyte, based on the parameters of the light source. The sensitivity of the plasmon sensor as a function of the period is shown in Fig. 4(a), with the diameter of the nano-disks kept at 280 nm. It can be observed that an increase in the periodicity leads to an increase in sensitivity. The RI sensitivity can reach 853 nm/RIU at a period of 900 nm. The FOM of the plasmon sensor as a function of the period is shown in Fig. 4(b). As the period increases, the FOM increases in non-linearity and a high value of FOM = 126 RIU^{-1} is achieved when the period is 900 nm. From the formula for the FOM, we can extract two explanations for this increase in the FOM: an increasing RI sensitivity and a decreasing FWHM. These two reasons are both related in this plasmon sensor.

It seems that we can get a higher sensitivity by applying a larger period, but in fact, as we continue to increase the period, mode 2 moves to a longer wavelength and ultimately interacts with mode 3. Reflection spectra for the same nano-disk diameter of 280 nm and background RI (analyte) of 1.30, with varied periods, are shown in Fig. 4(c). Figure 4(b) clearly indicates that mode 2 is sensitive to the period, whereas mode 3 barely changes. It also clearly demonstrates how mode 2 interacts with mode 3, when mode 2 and mode 3 have almost the same resonance wavelength. If we continue to increase the period, an anti-crossing behavior can be observed from the spectra.[54] As shown by the blue dashed line in Fig. 4(c), when the period reaches 1100 nm, the FWHM of mode 2 is obviously increasing, and the reflectivity is not close to zero, unlike for other periods under 1100 nm. The same problem becomes more palpable when we increase the period to 1150 nm, as shown by the solid black line in Fig. 4(c). In others words, when modes 2 and 3 interact with each other, the advantages of mode 2 for RI sensing (low reflectivity and a narrow FWHM) are lost. Accordingly, although increasing the period can bring higher RI sensitivity, this structure does not provide the same advantages as a plasmonic RI sensor when the period is too large.

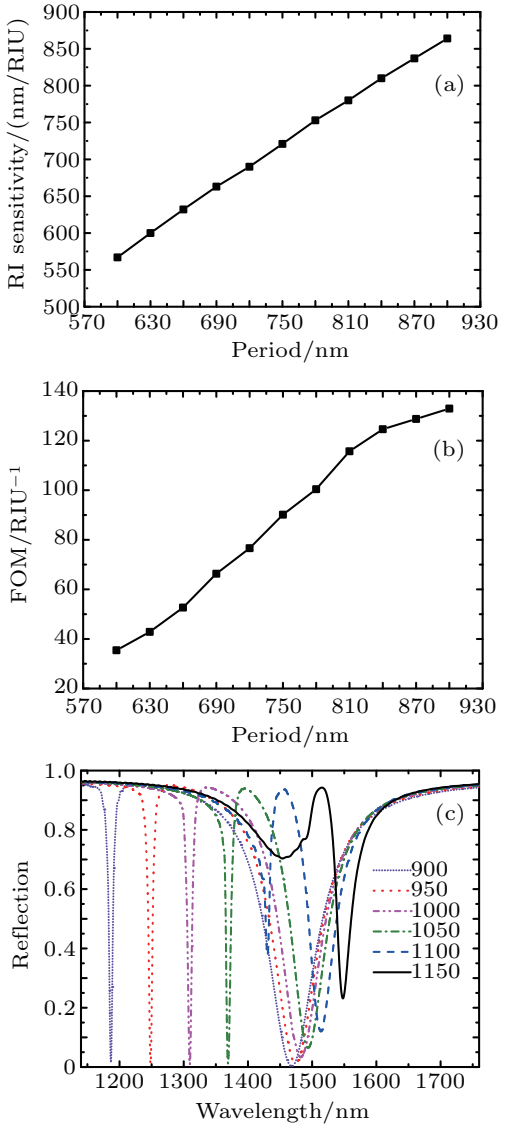


Fig. 4. (a) The RI sensitivity as a function of the period, with the period varying from 600 nm to 900 nm in step sizes of 30 nm. (b) The FOM as a function of the period. (c) The reflection spectra of the composite structure with a period range from 900 nm to 1150 nm, step size of 50 nm, background RI (analyte) of 1.3, and nano-disk diameter of 280 nm.

3.4. Influence of the diameter on the sensitivity and FOM

Another important geometric parameter of this structure is the diameter of the nano-disks. With the period fixed at 720 nm, the RI sensitivity as a function of the diameter of the nano-disks is shown in Fig. 5(a), with the diameter of the nano-disks increasing from 200 nm to 360 nm, in step sizes of 20 nm. A slight fluctuation in the RI sensitivity can be observed, but ultimately the diameter of the nano-disks has little effect on the RI sensitivity. This further demonstrates that our structure can work as a plasmonic RI sensor even in a relatively rough process. Figure 5(b) shows the FOM as a function of the diameter of the nano-disks. The FOM reaches the highest value of 85 RIU^{-1} when the diameter of the nano-disks is 240 nm. This may be attributed to the enhancement factor reaching a maximum when the diameter is 240 nm.[55] Strong resonance leads to a narrow FWHM and a high FOM.

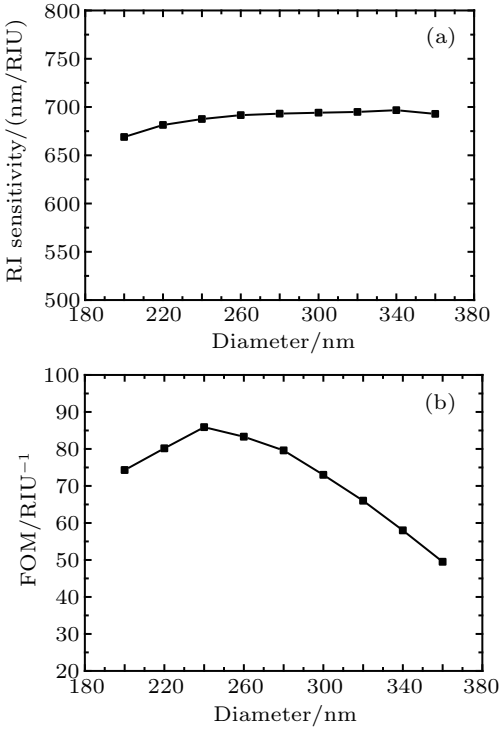


Fig. 5. (a) The RI sensitivity as a function of nano-disk diameter, where the diameter varies from 200 nm to 360 nm, in step sizes of 20 nm. (b) The FOM as a function of the nano-disk diameter, where the diameter varies from 200 nm to 360 nm, in step sizes of 20 nm.

4. Conclusions

In summary, we proposed a plasmonic RI sensor based on a gold composite structure. According to numerical simulations, the proposed design exhibits a good linear relationship between the resonance mode and the RI of the analyte, indicating favorable sensing performance. By analyzing the geometric parameters of the structure, we find that our sensor is quite flexible in terms of the period and the diameters of the nano-disks. Our sensor has a good sensitivity and FOM in a large period and diameter range, and it is convenient for practical application. The sensitivity and the FOM are of high values compared with those in previously reported work. With a 900-nm period and 280-nm diameter for the nano-disk array, we obtained an achievable RI sensitivity of 853 nm/RIU and an FOM of 126 RIU^{-1}. Our structure could provide a good reference for plasmonic sensors and could be widely used in biological and chemical sensing.

References

[1] Hou W and Cronin S B 2013 *Adv. Funct. Mater.* **23** 1612
[2] Yan Y, Yang H, Zhao X, Li R and Wang X 2018 *Mater. Res. Bull.* **105** 286
[3] Zhao X, Yang H, Li S, Cui Z and Zhang C 2018 *Mater. Res. Bull.* **107** 180
[4] Zheng C and Yang H 2018 *J. Mater. Sci. Mater. Electron.* **29** 9291
[5] Ye Y, Yang H, Zhang H and Jiang J 2018 *Environ. Technol.*
[6] Chen Y, Wang X, Wang R, Yang H and Qi Y 2017 *Chin. Phys. B* **26** 054203
[7] Wang X, Tong H, Pang Z, Zhu J, Wu X, Yang H and Qi Y 2019 *Opt. Quantum Electron.* **51** 38
[8] Pang Z, Tong H, Wu X, Zhu J, Wang X, Yang H and Qi Y 2018 *Opt. Quantum Electron.* **50** 335
[9] Yang Z J, Jiang R, Zhuo X, Xie Y M, Wang J and Lin H Q 2017 *Phys. Rep.* **701** 1
[10] Wang J, Lu C, Hu Z, Chen C, Pan L and Ding W 2018 *Opt. Express* **26** 23221
[11] Chen J, Yi Z, Xiao S and Xu X 2018 *Mater. Res. Express* **5** 015605
[12] Liu L, Chen J, Zhou Z, Yi Z and Ye X 2018 *Mater. Res. Express* **5** 045802
[13] Yu M, Huang Z, Liu Z, Chen J, Liu Y, Tang L and Liu G 2018 *Sens. Actuators B Chem.* **262** 845
[14] Liu G, Yu M, Liu Z, Liu X and Huang S 2015 *Nanotechnology* **26** 185702
[15] Wang X, Bai X, Pang Z, Yang H, Qi Y and Wen X 2019 *Acta Phys. Sin.* **68** 037301 (in Chinese)
[16] Du H, Zhang L and Li D 2018 *Plasma Sci. Technol. Pap.* **20** 115001
[17] Li D, Zhang L and Du H 2019 *Plasma Sci. Technol.* **21** 045002
[18] Safari S and Jazi B 2018 *Plasmonics* **13** 1449
[19] Cennamo N, D'Agostino G, Donà A, Dacarro G, Pallavicini P, Pesavento M and Zeni L 2013 *Sens. (Switzerland)* **13** 14676
[20] Law W, Yong K, Baev A and Prasad P N 2011 *ACS Nano* **5** 4858
[21] Petryayeva E and Krull U J 2011 *Anal. Chim. Acta* **706** 8
[22] Kim J A, Hwang T, Dugasani S R, Amin R, Kulkarni A, Park S H and Kim T 2013 *Sens. Actuators B Chem.* **187** 426
[23] Qu S, Song C, Xia X, Liang X, Tang B, Hu Z and Wang J 2016 *Sensors* **16** 784
[24] Liu C, Wang F, Lv J, Sun T, Liu Q, Fu C, Mu H and Chu P K 2016 *Opt. Commun.* **359** 378
[25] Wang F, Sun Z, Sun T, Liu C, Chu P K and Bao L 2018 *J. Opt.* **47** 288
[26] Im H, Shao H, Il Y, Peterson V M, Castro C M, Weissleder R and Lee H 2014 *Nat. Biotechnol.* **32** 490
[27] Pallarola D, Schneckenburger M, Spatz J P and Pacholski C 2013 *Chem. Commun.* **49** 8326
[28] Coskun A F, Cetin A E, Galarreta B C, Alvarez D A, Altug H and Ozcan A 2014 *Sci. Rep.* **4** 6789
[29] Wang X, Bai X, Pang Z, Yang H and Qi Y 2019 *Results Phys.* **12** 1866
[30] Li J, Zhao Y, Hu H, Wang Q and Zhang J 2015 *Optik (Stuttg).* **126** 199
[31] Wang X, Wu X, Chen Y, Bai X, Pang Z, Yang H, Qi Y and Wen X 2018 *AIP Adv.* **8** 105029
[32] Byun K M, Kim S J and Kim D 2007 *Appl. Opt.* **46** 5703
[33] Mayer K M, Hafner J H and À A 2011 *Chem. Rev.* **111** 3828
[34] Nusz G J, Marinakos S M, Curry A C, Dahlin A, Höök F, Wax A and Chilkoti A 2008 *Anal. Chem.* **80** 984
[35] Dondapati S K, Sau T K, Hrelescu C, Klar T A, Stefani F D and Feldmann J 2010 *ACS Nano* **4** 6318
[36] Huang C, Ye J, Wang S, Stakenborg T and Lagae L 2012 *Appl. Phys. Lett.* **100** 173114

[37] Zhang Z, Wang L, Hu H, Li K, Ma X and Song G 2013 *Chin. Phys. B* **22** 104213
[38] Wang S, Sun X, Ding M, Peng G, Qi Y, Wang Y and Ren J 2018 *J. Phys. D: Appl. Phys.* **51** 405101
[39] Chen J, Fan W, Zhang T, Tang C, Chen X, Wu J, Li D and Yu Y 2017 *Opt. Express* **25** 3675
[40] Chen J, Zhang T, Tang C, Mao P, Liu Y, Yu Y and Liu Z 2016 *IEEE Photon. Technol. Lett.* **28** 1529
[41] Cen C, Chen J, Liang C, Huang J, Chen X, Tang Y, Yi Z, Xu X, Yi Y and Xiao S 2018 *Physica E* **103** 93
[42] Zhang X, Qi Y, Zhou P, Gong H, Hu B and Yan C 2018 *Photonic Sens.* **8** 367
[43] Qi Y, Zhang X, Zhou P, Hu B and Wang X 2018 *Acta Phys. Sin.* **67** 197301 (in Chinese)
[44] Wang J, Sun L, Hu Z, Liang X and Liu C 2014 *AIP Adv.* **4** 123006
[45] Wang J, Song C, Hang J, Hu Z and Zhang F 2017 *Opt. Express* **25** 23880
[46] Cen Chunlian, Lin H, Huang J, Liang C, Chen X, Tang Y, Yi Z, Ye X, Liu J, Yi Y and Xiao S 2018 *Sensors* **18** 4489
[47] Liang C, Niu G, Chen X, Zhou Z, Yi Z, Ye X, Duan T, Yi Y and Xiao S 2019 *Opt. Commun.* **436** 57
[48] Liu Z, Liu G, Huang S, Liu X, Pan P, Wang Y and Gu G 2015 *Sens. Actuators B Chem.* **215** 480
[49] Yang Z J 2016 *J. Phys. Chem. C* **120** 21843
[50] Yang Z J , Zhao Q and He J 2017 *Opt. Express* **25** 15927
[51] Johnson P B and Christy R W 1972 *Phys. Rev. B* **6** 4370
[52] Yi Z, Liu M, Luo J, Zhao Y, Zhang W, Yi Y, Yi Y, Duan T, Wang C and Tang Y 2017 *Opt. Commun.* **390** 1
[53] Cesario J 2005 *Opt. Lett.* **30** 3404
[54] Chu Y and Crozier K B 2009 *Opt. Lett.* **34** 244
[55] Zhou F, Liu Y and Cai W 2014 *Opt. Lett.* **39** 1302